Rev. Adv. Mater. Sci. 47 (2016) 1-8

PLASTIC DEFORMATION THROUGH DE-TWINNING MEDIATED BY INCOHERENT TWIN BOUNDARIES IN NANOTWINNED METALLIC ALLOYS

I.A. Ovid'ko[1,2,3] and A.G. Sheinerman[1,2,3]

[1]Research Laboratory for Mechanics of New Nanomaterials,
Peter the Great St. Petersburg Polytechnic University, St. Petersburg 195251, Russia
[2]Saint Petersburg State University, 7/9 Universitetskaya nab., St. Petersburg, 199034 Russia
[3]Institute of Problems of Mechanical Engineering, Russian Academy of Sciences,
Bolshoj 61, Vasilievskii Ostrov, St. Petersburg 199178, Russia

Received: September 7, 2016

Abstract. We suggest a theoretical model that describes the effects of solute atoms on plastic deformation through de-twinning processes mediated by incoherent twin boundaries (ITBs) in nanotwinned metallic alloys under a mechanical load. Within the model, the regions near ITBs contain the segregations of solute atoms formed during the fabrication of nanotwinned alloys in the stress fields of the dislocations composing ITBs. The critical parameters are calculated which characterize de-twinning processes in Cu-based nanotwinned alloys containing low concentrations of Ni, Zn or Al. By comparison of these critical parameters with those specifying pure nanotwinned Cu, it is concluded that solute atoms can effectively strengthen nanotwinned alloys.

1. INTRODUCTION

Nanostructured materials show outstanding mechanical properties due to the nanoscale and interface effects causing operation of specific deformation mechanisms in these materials; see, e.g., [1–23]. In recent years, a rapidly growing interest has been devoted to nanotwinned metals – nanostructured metals containing high densities of nanoscale twins – that often show concurrent superior strength and good ductility [24,45]. This unique combination of the key mechanical characteristics exhibited by nanotwinned metals is closely related to specific deformation mechanisms operating in them. In particular, such micromechanisms include plastic deformation through the motion of partial dislocations along coherent twin boundaries (CTBs) and associated widening/narrowing of nanoscale twins [30,35,37,41,45], deformation mediated by partial dislocations that slide along crystal planes inclined to CTBs and are hampered at such boundaries [25,26,34], deformation mediated by threading partial dislocations that slide in twin interiors in the direction parallel to CTBs [41,46], and plastic deformation through de-twinning mediated by incoherent twin boundaries (ITBs) migrating under stress [29,38].

Note that previous research of the mechanical properties of nanotwinned metallic materials addressed pure metals with nanotwinned structures (see reviews [28,42–44]), but not metallic alloys. At the same time, the deformation behavior of conventional ultrafine-grained materials (without a nanotwinned structure) is well-known to be highly sensitive to alloying; see, e,g,. [47,48]. Besides, recently, computer simulations [49] have demonstrated that solute Ag atoms can significantly improve the thermal stability of nanotwinned structures

Corresponding author: I.A. Ovid'ko, e-mail: ovidko@gmail.com

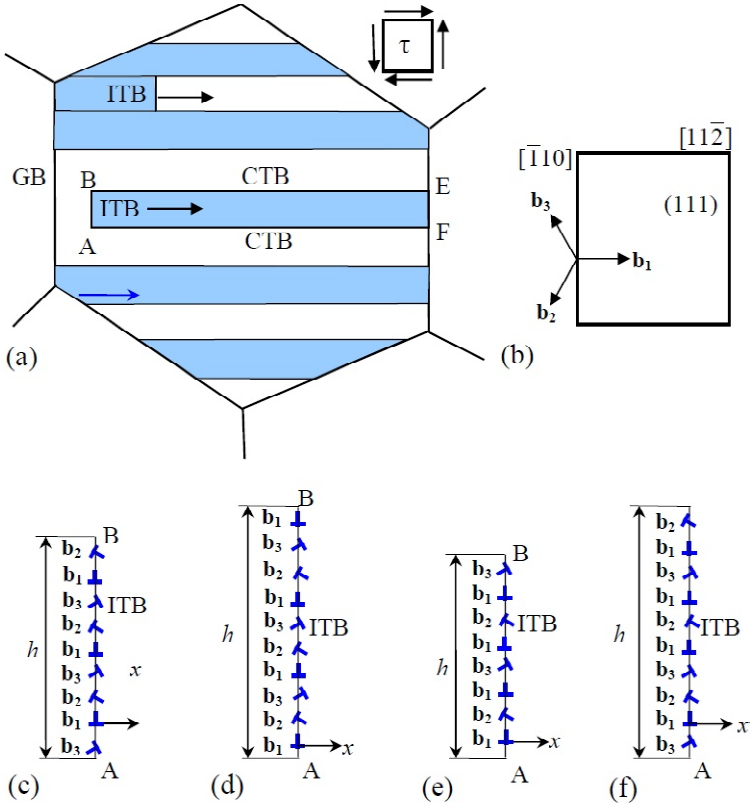

Fig. 1. De-twinning in a deformed nanotwinned solid. (a) A grain of a nanotwinned solid under the action of an applied shear stress τ . An incoherent twin boundary (ITB) moves under the action of the applied shear stress along coherent twin boundaries (CTBs). (b) Geometry of dislocations composing the ITB. (c–f) Dislocation structures of ITBs.

in nanotwinned Cu-Ag alloy. Also, various binary nanotwinned Cu-Ni and Cu-Al alloys with controlled twin thicknesses have recently been fabricated by magnetron sputtering [50]. In the context discussed, it is highly interesting to fully understand the effects of alloying on the plastic deformation processes occurring in nanotwinned metallic materials. The main aim of this paper is to theoretically examine and describe the effects of solute atoms on plastic deformation through de-twinning mediated by ITBs that migrate in nanotwinned alloys under mechanical stresses. In doing so, we will focus our theoretical examination on plastic deformation through de-twinning in Cu-based nanotwinned alloys containing low concentrations of Ni, Zn or Al.

2. DE-TWINNING DEFORMATION THROUGH THE STRESS-DRIVEN MIGRATION OF INCOHERENT TWIN BOUNDARIES IN NANOTWINNED METALLIC ALLOYS. GEOMETRIC ASPECTS

Let us consider plastic flow through de-twinning in a grain of a deformed nanotwinned binary alloy with a face-centered cubic (fcc) lattice (Fig. 1a). Within our model, the grain contains many nanoscale growth twins divided by CTBs. We assume that an applied shear stress τ acts in the examined grain as shown in Fig. 1a. In the initial state, the grain contains a rectangular twin ABEF bounded by GB segment EF, CTBs CE and BF and an ITB AB (Fig. 1a). We now examine the situation where the ITB AB moves along the CTBs BE and AF (Fig. 1a) and its motion is accompanied by the shrinkage of the CTB fragments AF and BE, thus leading to the shrinking of the twin AFEB. If the ITB AB approaches the GB EF, the twin AFEB completely disappears, thus promoting de-twinning of the nanotwinned solid.

We now consider the geometric features of the ITB AB. In fcc solids, CTBs typically lie in {111} crystal planes, while ITBs are located in {112} planes. For definiteness, we suppose that CTBs AF and BE lie in (111) crystal planes, while the ITB AB is located in a (11$\bar{2}$) crystal plane. Within our model, following Refs. [29,51], the stress-driven motion of the (11$\bar{2}$) ITB and the associated shrinkage of the CTBs BE and AF occur through the simultaneous motion of the Shockley partial dislocations along all the (111) planes of the twin AFEB. Each Shockley

partial dislocation has the line direction $[\bar{1}10]$ and one of Burgers vectors, $\boldsymbol{b}_1$, $\boldsymbol{b}_2$ or $\boldsymbol{b}_3$, where,$\boldsymbol{b}_1 = (a/6)[11\bar{2}]$, $\boldsymbol{b}_2 = (a/6)[1\bar{2}1]$ and $\boldsymbol{b}_3 = (a/6)[\bar{2}11]$ (Fig. 1b), with a being the crystal lattice parameter. The dislocations specified by the Burgers vector $\boldsymbol{b}_1$ represent edge dislocations, whereas those with the Burgers vectors $\boldsymbol{b}_2$ and $\boldsymbol{b}_3$ are 30° mixed dislocations. The vector sum of the three Burgers vectors $\boldsymbol{b}_1$, $\boldsymbol{b}_2$, and $\boldsymbol{b}_3$ is zero: $\boldsymbol{b}_1+\boldsymbol{b}_2+\boldsymbol{b}_3=0$. Various configurations of these dislocations form ITBs that can mediate plastic flow in nanotwinned metals [38]. We will consider the examples of such configurations and their characteristics in next section.

3. CRITICAL PARAMETERS FOR PLASTIC DEFORMATION THROUGH DE-TWINNING IN NANOTWINNED FCC ALLOYS

Let us calculate the critical parameters that specify plastic deformation through de-twinning (Fig. 1) in nanotwinned fcc alloys. For definiteness, we will focus our examination on binary solid solutions having a low atomic content of one of its constituent metals, as compared to another (dominating) constituent metal. The atoms of the former metal in a binary metallic alloy will be called solute atoms.

Also, note that nanotwinned metallic materials are typically fabricated at highly non-equilibrium conditions (electrodeposition, magnetron sputtering), so that intensive atomic diffusion occurs in these materials during their synthesis. In the case of alloys, solute atoms diffuse in the spatially inhomogeneous stress fields created by defects, in particular, dislocations at ITBs. The diffusion affected by ITB dislocations results in the spatially inhomogeneous distributions of solute atoms near ITBs. For definiteness, we address the situation where the distribution of solute atoms in a nanotwinned alloy approaches the equilibrium one.

We now examine the dislocation configurations of ITBs in nanotwinned metals. First, let us consider the situation where the ITB dislocations form a periodic structure with the zero total Burgers vector, as shown in Fig. 1c. In this situation, stress-driven migration of the ITB does not contribute to plastic flow but modifies the nanotwinned structure of a metal. In the case shown in Fig. 1c, we calculate the projection F_x of the force F acting on the moving ITB (per unit boundary length in the direction normal to the plane of Figs. 1c). The force projection F_x is given as

$$F_x = F_x^{sol} - (h/p)b\tau_p^e + 2\gamma_{CTB}, \qquad (1)$$

where F_x^{sol} is the projection of the force acting on the ITB due to solute atoms, γ_{CTB} is the specific (per unit area) energy of the CTB, τ_p^e is the mean Peierls stress acting on the ITB dislocations, h is the ITB length, and $p=a/\sqrt{3}$ is the distance between the neighboring (111) crystal planes. The force projection F_x^{sol} is calculated in Appendix A. Our calculations demonstrated that F_x^{sol} decreases with the distance x_0 moved by the ITB. We assume that the dislocations belonging to the ITB can pass the distance $x' = \sqrt{6}\,a/2$ along the x-axis by thermal fluctuations. (This is equivalent to the motion of the dislocations along their slip direction $[01\bar{1}]$ by the distance $\sqrt{2}a$, that is by two interatomic distances.) Then the condition for the ITB migration can be written as $F_x(x_0=x')>0$. Using the relation $p/b = \sqrt{2}$, the latter condition can be written as $h<h_c$, where

$$h_c = \frac{\sqrt{2}\left(F_x^{sol}(x_0 = x') + 2\gamma_{CTB}\right)}{\tau_p^e}. \qquad (2)$$

The parameter h_c appearing in formula (2) represents the critical twin thickness below which the twin becomes unstable relative to de-twinning via ITB migration. In the case of a pure nanotwinned metal, where $F_x^{sol}=0$, the relation $h<h_c$ is reduced to the relation $h<h_{c0}$, where $h_{c0}=2\sqrt{2}\gamma_{CTB}/\tau_p^e$. Here h_{c0} is the critical twin thickness for a nanotwinned metal.

Let us calculate the critical thickness h_c in the case of Cu-Ni, Cu-Zn, and Cu-Al nanotwinned fcc alloys with 2 at.% of Ni, Zn and Al, respectively, and compare it with the critical twin thickness h_{c0} in the case of pure nanotwinned Cu. The Cu-Ni, Cu-Zn and Cu-Al alloys are characterized by the following values of the shear modulus G, Poisson's ratio ν, crystal lattice parameter a, atomic volume V_{at}: G=48 GPa, ν=0.34, $a\approx$0.36 nm, and V_{at} = 1.18 10^{-29} m^3. Also, we put T=300K (where T is the temperature) and τ_p^e=15 MPa. Besides, we have: ε=-0.033, for the Cu-Ni alloy [52]; ε=-0.05, for the Cu-Zn alloy [53,54]; and ε=-0.07, for the Cu-Al alloy [55], where $\varepsilon = (1/a)/(\partial a/\partial c_0)$, $a(c_0)$ is the mean lattice constant that characterizes Cu-Ni, Cu-Zn, and Cu-Al alloys and depends on the solute concentration c_0. For the above parameters, from formula (2) and the equations for the force F_x^{sol}, we obtain: h_c=2.5 nm, for Cu-Ni; h_c=1.25 nm, for Cu-Zn and Cu-Al; and h_{c0}=4.5 nm. These values are indicative of the fact that the presence of Ni, Zn or Al solute atoms significantly reduces the critical twin thickness.

We now examine the situations where the total Burgers vector of the ITB dislocations is not equal to zero. In doing so, stress-driven migration of ITB

contributes to plastic flow in a nanotwinned material. For definiteness, first, we consider the case where the ITB dislocations form a periodic structure shown in Fig. 1d, and the total Burgers vector of the ITB dislocations is equal to $\boldsymbol{b}_1$. In this case, the projection $\tilde{F}_x$ of the total force, acting on the ITB, on the x-axis can be written as

$$\tilde{F}_x = \tilde{F}_x^{sol} + \tau b - (h/p) b \tau_p^e + 2\gamma_{CTB}, \quad (3)$$

where $\tilde{F}_x^{sol}$ is the projection of the force acting on the ITB due to solute atoms for the arrangement of the ITB dislocations shown in Fig. 1d. The expressions for the force $\tilde{F}_x^{sol}$ are obtained in the same way as those for the force F_x^{sol} (see Appendix A). The calculations demonstrate that, similar to the force F_x, the force $\tilde{F}_x$ decreases with increasing the distance x_0 moved by the ITB. Therefore, we can write the condition for the ITB migration as $\tilde{F}_x(x_0=x')>0$, where $x'=\sqrt{6}a/2$, as above.

Using formula (3), the relation $\tilde{F}_x(x_0=x')>0$ can be presented as $\tau>\tau_c$, where

$$\tau_c = -\frac{\tilde{F}_x^{sol}(x_0 = x')}{b} + \frac{h\tau_p^e}{p} - \frac{2\gamma_{CTB}}{b}. \quad (4)$$

In the case of a nanotwinned metal, where $c_0=0$ and $\tilde{F}_x^{sol}=0$, we have:

$$\tau_c(c_0 = 0) = \left(h\tau_p^e - 2\sqrt{2}\gamma_{CTB}\right)/p.$$

The dependences of the critical stress τ_c (beyond which the twin stops to be stable) on twin thickness h are shown in Fig. 2a for Cu-Ni, Cu-Zn, and Cu-Al alloys with 2 at.% of Ni, Zn or Al. The dashed line in Fig. 2a also illustrates the dependence $\tau_c(h)$ for nanotwinned Cu. Fig. 2a demonstrates that τ_c increases with twin thickness h, and the values of τ_c for Cu alloys are always higher than those for pure Cu. For the case of the Cu-Al alloy, the values of τ_c are very high for any values of h, which implies that the Cu-Al alloy should be stable with respect to detwinning at any realistic values of the applied load and twin thickness. For the Cu-Ni and Cu-Zn alloys, the realistic values of flow stress τ=0.3 GPa (shown by the horizontal dotted line in Fig. 2a) corresponds to the twin thickness intervals (at which the twin becomes unstable during deformation) h<3.5 nm and h<1.5 nm, respectively, while for pure Cu, at τ=0.3 GPa, the twin is unstable at h<8.5 nm (Fig. 2a).

We now consider the situation where the ITB is highly non-equilibrium and contains a comparatively large dislocation charge, so that ITB migration significantly contributes to plastic flow. In this situation, the ITB is assumed to consist of periodically arranged structural units characterized by non-zero Burgers vectors. In the case illustrated in Fig. 1e (where two structural units are depicted), each structural unit contains four dislocations (with the Burgers vectors $\boldsymbol{b}_1$, $\boldsymbol{b}_2$, $\boldsymbol{b}_1$ and $\boldsymbol{b}_3$). In this case, the magnitude of the total dislocation Burgers vector per unit ITB length is $b/(4p)$. In the situation presented in Fig. 1f (where one structural unit is shown), each structural unit comprises 10 dislocations, and the ITB fragment containing one such unit has the total Burgers vector $\boldsymbol{b}_1$. In this case, the magnitude of

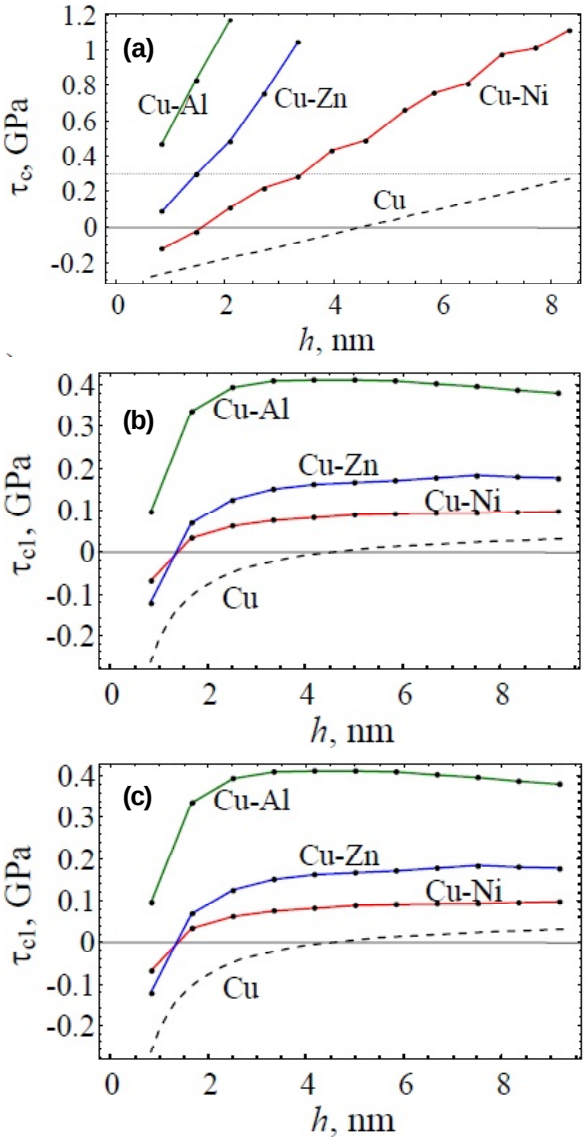

Fig. 2. Dependences of the critical shear stress τ_c (a) and τ_{c1} (b,c), for Cu-Ni, Cu-Zn and Cu-Al alloys on twin thickness h, in the situations where de-twinning occurs through migration of ITBs with the dislocation structures illustrated in Fig. 1d (a), 1e (b), and 1f (c). The dashed lines show the dependences $\tau_c(h)$ and $\tau_{c1}(h)$, for pure nanotwinned Cu.

the total dislocation Burgers vector per unit ITB length is $b/(10p)$.

In the situations shown in Figs. 1e and 1f, the projection F_{1X} of the total force, acting on the ITB, on the x-axis can be written as

$$F_{1x} = F_{1x}^{sol} + bh\left(\tau - n\tau_p^e\right)/\left(np\right) + 2\gamma_{CTB}, \qquad (5)$$

where F_{1x}^{sol} is the projection of the force acting on the ITB due to solute atoms for the arrangement of the ITB dislocations shown in Figs. 1e and 1f, and n is the number of dislocations in the structural unit (n =4 and n =10 in the cases shown in Figs. 1e and 1f, respectively). Using formula (5), the condition $F_1(x_0=x')>0$ for ITB migration can be presented as $\tau>\tau_{c1}$, where

$$\tau_{c1} = -\frac{\left(F_{1x}^{sol}(x_0 = x') + 2\gamma_{CTB}\right)}{bh} + n\tau_p^e. \qquad (6)$$

The expressions for the force F_{1x}^{sol}, for the ITB structures shown in Figs. 1e and 1f, are derived in the same way as the expressions for the force F_{1x}^{sol}. Using these expressions, we have calculated the dependences $\tau_{c1}(h)$, for Cu-Ni, Cu-Zn, and Cu-Al alloys with 2 at.% of Ni, Zn, and Al, respectively. These dependences are plotted in Figs. 2b and 2c, for the ITB dislocation structures illustrated in Figs. 1e and 1f, respectively. Figs. 2b and 2c demonstrate that, as with the case shown in Fig. 2a, the values of τ_{c1} for Cu alloys are always higher than those for pure Cu. In particular, for pure nanotwinned Cu, the critical stress for de-twinning of twins with the non-equilibrium ITBs illustrated in Figs. 1e and 1f does not exceed 100 MPa, when twin thickness is less than 10 nm. At the same time, the critical stress τ_{c1} for de-twinning processes in Cu alloys increases dramatically, as compared to the case of pure Cu. For instance, in the case of the Cu-Al alloy, the critical stress τ_{c1} is around 0.4 GPa, for the ITB shown in Fig. 1e, and exceeds 1 GPa, for the ITB presented in Fig. 1f. Also, for a specified twin thickness h, the corresponding values of τ_{c1} for Cu-Al are higher than those for Cu-Zn, and the values of τ_{c1} for Cu-Zn are higher than those for Cu-Ni. This trend is associated with the differences in the absolute value of the parameter ε (that determines the internal stresses created by the solid solution) for these three alloys.

Figs. 2b and 2c also demonstrate that the critical stress τ_{c1} for Cu-Al and Cu-Zn first increases and then decreases with increasing h, in contrast to the critical stress τ_{c1} for pure Cu and Cu-Ni, which monotonously increases with h. Apparently, this behavior is associated with the effects of the ITB edges, resulting in the fact that the absolute value, $-F_{1x}^{sol}/h$, of the force exerted by the solid solution on ITB of unit length decreases with h for small enough twin thicknesses. As a result, the term $-npF_{1x}^{sol}(x_0=x')/(bh)$ appearing in formula (6) for τ_{c1} decreases with h and, if the values of this term are large enough, may result in decreasing of τ_{c1} with increasing h.

4. CONCLUDING REMARKS

To summarize, nanotwinned alloys containing the equilibrium atmospheres of solute atoms around ITBs are more stable relative to de-twinning through ITB migration, as compared to pure nanotwinned metals. The main parameter that determines the ability of solute atoms to stabilize the nanotwinned structure is the parameter ε that describes variation in the crystal lattice parameter of a nanotwinned alloy due to change in atomic concentration of solute atoms. An increase in ε enhances the stability of nanotwinned binary alloys relative to de-twinning.

Also, stress-induced migration of non-equilibrium ITBs (Figs. 1e and 1f) mediates plastic deformation in nanotwinned solids. If the fraction of non-equilibrium ITBs is sufficiently high, this plastic deformation mechanism can considerably contribute to the overall plastic deformation of the nanotwinned solid. In the latter case, when the critical stress τ_{c1} increases due to solute atoms, so do both the yield and flow stresses. As a corollary, solute atoms can effectively strengthen nanotwinned metallic alloys, as compared to their pure metal counterparts.

APPENDIX A: THE FORCE EXERTED ON AN INCOHERENT TWIN BOUNDARY BY A BINARY SOLID SOLUTION

In this Appendix, we calculate the force F_x^{sol} exerted by a binary solid solution on the incoherent twin boundary with the dislocation structure shown in Fig. 1c. To do so, let us assume that under the action of the shear stress τ the ITB has moved from the plane x=0 of the Cartesian coordinate system (Fig. A1a) to the plane $x=x_0$ (Fig. A1b). We also assume that diffusion has not enough time to occur during the ITB motion to the plane $x=x_0$, and the solute concentration corresponds to the equilibrium solute concentration in a solid with the ITB located in the plane x=0. Then the force projection F_x^{sol} acting on the ITB (per unit length of the dislocations composing the ITB) is calculated as $F_x^{sol}=-\partial W_{int}/\partial x_0$, where W_{int} is the total energy (per unit dislocation

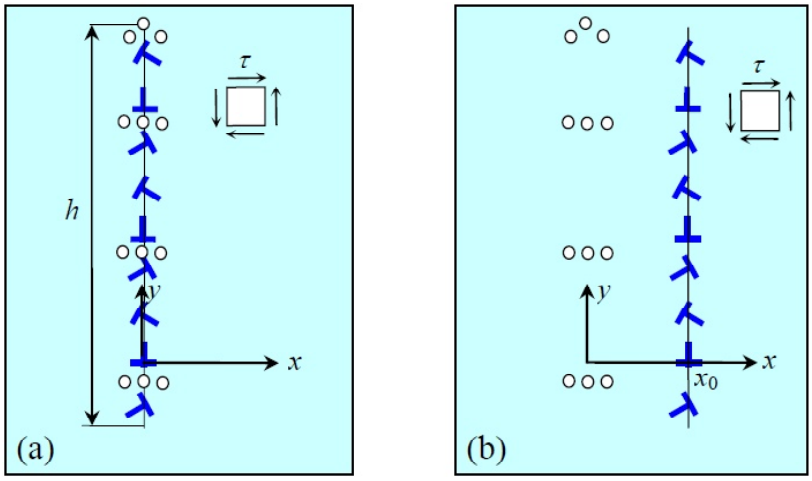

Fig. A1. ITB in a binary alloy. The white circles depict solute atoms near the dislocations composing the ITB. (a) The ITB is located in the plane x=0. (b) The ITB moves along the x-axis. The concentration profile of solute atoms does not change.

length) of the interaction of all the dislocations composing the ITB with the stress field created by the inhomogeneous distribution of solute atoms in the vicinity of the ITB.

In order to calculate the force exerted on the ITB by a binary solid solution, we model the solution as an isotropic solid with the shear modulus G and Poisson's ratio ν and calculate the equilibrium atomic concentration c of solute atoms at and near the examined ITB. To do so, we will use the equation [56]

$$\ln\frac{c}{1-c}-\ln\frac{c_0}{1-c_0}=\frac{3\sigma(x,y)\varepsilon V_{at}}{k_BT}, \tag{A1}$$

where c is the local atomic concentration of solute atoms, c_0 is the average atomic concentration of solute atoms, k_B is the Boltzmann constant, T is the absolute temperature, V_{at} is the average volume per atom, $\sigma(x,y)=(\sigma_{xx}+\sigma_{yy}+\sigma_{zz})/3$, σ_{xx}, σ_{yy}, and σ_{zz} are the components of the stress field σ_{ij} created by all the dislocations composing the ITB (Fig. A1a) prior to its migration in the Cartesian coordinate system (x,y,z) whose plane (x,y) is shown in Fig. A1, $\varepsilon = (1/a)/(\partial a/\partial c_0)$, and a is the average lattice constant of the binary alloy. From formula (A1), one obtains:

$$c(x,y)=\frac{c_0e^{\frac{3\sigma(x,y)V_{at}\varepsilon}{k_BT}}}{1-c_0+c_0e^{\frac{3\sigma(x,y)V_{at}\varepsilon}{k_BT}}}. \tag{A2}$$

The examined ITB with the dislocation configuration shown in Fig. 1c is composed of N triplets of the dislocations with the Burgers vectors $\boldsymbol{b}_1$, $\boldsymbol{b}_2$, and $\boldsymbol{b}_3$, and its length h is related to the number N of triplets and dislocation separation p as h=3Np. For such an ITB, from the expressions [56] for the stress fields of dislocations in an isotropic infinite solid, we have:

$$\sigma(x,y)=-\frac{Gb(1+\nu)}{6\pi(1-\nu)}\sum_{l=1}^{N}\big[2f(x,y-3pl)- f(x,y-p-3pl)-f(x,y+p-3pl)\big], \tag{A3}$$

where $f(x,y)=y/(x^2+y^2)$. After migration to the plane $x=x_0$, the ITB creates the dilatational stress $\sigma(x-x_0,y)$. Hence, the energy W_{int} (per unit dislocation length) of the elastic interaction of the dislocations with the stress field created by the inhomogeneous distributions of solute atoms can be written as [57]

$$W_{int}=-3\varepsilon\iint\limits_{(x-x_0)^2+y^2<R^2}\sigma(x-x_0,y)\times\big(c(x,y)-c_0\big)\,dx\,dy, \tag{A4}$$

where R is the screening length of the dislocation stress field (R>>(x_0,Np)). From formula (A4) and the relation $F_x^{sol}=-\partial W_{int}/\partial x_0$, one obtains:

$$F_x^{sol}=-3\varepsilon\iint\limits_{x^2+y^2<R^2}\sigma(x,y)\frac{\partial c(x+x_0,y)}{\partial x_0}\,dx\,dy. \tag{A5}$$

It should be noted that for R>>(x_0,Np), F_x^{sol} does not depend on R, so that in formula (A5), one can put $R\to\infty$. Then substitution of formula (A3) and the relation $f(x,y)=y/(x^2+y^2)$ to (A5) and a change of variable yields:

$$F_x^{sol} = \frac{Gb\varepsilon(1+\nu)}{2\pi(1-\nu)} \int_{-\infty}^{\infty}\int_{-\infty}^{\infty} \frac{y}{x^2+y^2} \times$$
$$\sum_{l=1}^{N} \frac{\partial}{\partial x_0} \big[2c(x+x_0, y+3pl) -$$
$$c(x+x_0, y+p+3pl) - \qquad \text{(A6)}$$
$$c(x+x_0, y-p+3pl)\big] \mathrm{d}x\, \mathrm{d}y.$$

Finally, by the change of variables $x=r\cos\varphi$, $y=r\sin\varphi$, formula (A6) can be rewritten as

$$F_x^{sol} = \frac{Gb\varepsilon(1+\nu)}{2\pi(1-\nu)} \times$$
$$\int_{-\pi}^{\pi}\int_{0}^{\infty} \frac{y}{x^2+y^2} \sum_{l=1}^{N} \frac{\partial}{\partial x_0} \times$$
$$\big[2c(r\cos\varphi + x_0, r\sin\varphi + 3pl) - \qquad \text{(A7)}$$
$$c(r\cos\varphi + x_0, r\sin\varphi + p + 3pl) -$$
$$c(r\cos\varphi + x_0, r\sin\varphi - p + 3pl)\big] \sin\varphi\, \mathrm{d}r\, \mathrm{d}\varphi.$$

Formulae (A2), (A3), and (A7) provide the expressions for the force F_x^{sol} exerted by a binary solid solution on the ITB shown in Fig. 1c.

ACKNOWLEDGEMENTS

The work was supported, in part (for IAO), by the Ministry of Education and Science of Russian Federation (Zadanie 9.1964.2014/K and grant 14.B25.31.0017) and St. Petersburg State University (grant 6.38.337.2015) and, in part (for AGS), by the Ministry of Education and Science of Russian Federation (grant MD-2893.2015.1) and the Russian Fund of Basic Research (grant 15-31-20095).

REFERENCES

[1] K.S. Kumar, S. Suresh and H. Van Swygenhoven // *Acta Mater* **51** (2003) 5743.
[2] D. Wolf, V. Yamakov, S.R. Phillpot, A.K. Mukherjee and H. Gleiter // *Acta Mater.* **53** (2005) 1.
[3] S.V. Bobylev, M.Yu. Gutkin and I.A. Ovid'ko // *Phys.Rev.* B **73** (2006) 064102.
[4] C.C. Koch // *J. Mater. Sci.* **42** (2007) 1403.
[5] M. Dao, L. Lu, R.J. Asaro, J.T.M. De Hosson and E. Ma // *Acta Mater.* **55** (2007) 4041.
[6] M.Yu. Gutkin and I.A. Ovid'ko // *Acta Mater.* **56** (2008) 1642.
[7] S.V. Bobylev, A.K. Mukherjee, I.A. Ovid'ko and A.G. Sheinerman // *Int. J. Plasticity* **26** (2010) 1629.
[8] J.R. Greer and J.T.M. De Hosson // *Prog. Mater. Sci.* **56** (2011) 654.
[9] Y.T. Zhu, X.Z. Liao and X.-L. Wu // *Prog. Mater. Sci.* **57** (2012) 1.
[10] R.Z. Valiev, I. Sabirov, A.P. Zhilyaev and T.G. Langdon // *JOM* **64** (2012) 1134.
[11] I.A. Ovidko and A.G. Sheinerman // *Rev. Adv. Mater. Sci.* **37** (2014) 97.
[12] A.A. Samigullina, A.A. Nazarov, R.R. Mulyukov, Yu.V. Tsarenko and V.V. Rubanik // *Rev. Adv. Mater. Sci.* **39** (2014) 48.
[13] B.N. Semenov, I.V. Smirnov, Yu.V. Sudenkov and N.V. Tatarinova // *Mater. Phys. Mech.* **24** (2015) 319.
[14] I.A. Ovid'ko and A.G. Sheinerman // *Rev. Adv. Mater. Sci.* **39** (2014) 99.
[15] E. Khafizova, R. Islamgaliev, G. Klevtsov and E. Merson // *Mater. Phys. Mech.* **24** (2015) 232.
[16] G.I. Raab, D.V. Gunderov, L.N. Shafigullin, Yu.M. Podrezov, M.I. Danylenko, N.K. Tsenev, R.N. Bakhtizin, G.N. Aleshin and A.G. Raab // *Mater. Phys. Mech*. **24** (2015) 242.
[17] A.E. Medvedev, M.Yu. Murashkin, N.A. Enikeev, I.A. Ovid'ko and R.Z. Valiev // *Mater. Phys. Mech.* **24** (2015) 297.
[18] Ya.V. Konakov, I.A. Ovid'ko and A.G. Sheinerman // *Mater. Phys. Mech.* **24** (2015) 97.
[19] V.D. Sitdikov, I.V. Alexandrov, M.M. Ganiev, E.I. Fakhretdinova and G.I. Raab // *Rev. Adv. Mater. Sci.* **41** (2015) 44.
[20] E.V. Bobruk, X. Sauvage, N.A. Enikeev, B.B. Straumal and R.Z. Valiev // *Rev. Adv. Mater. Sci*. **43** (2015) 45.
[21] M.M. Abramova, N.A. Enikeev, X. Sauvage, A. Etienne, B. Radiguet, E. Ubyivovk and R.Z. Valiev // *Rev. Adv. Mater. Sci.* **43** (2015) 83.
[22] P.Kumar, M. Kawasaki and T.G. Langdon // *J. Mater. Sci.* **51** (2016) 7.
[23] M. Kawasaki and T.G. Langdon // *J. Mater. Sci.* **51** (2016) 19.
[24] L. Lu, Y. Shen, X. Chen, L. Qian and K. Lu // *Science* **304** (2004) 422.
[25] T. Zhu, J. Li, A. Samanta, H.G. Kim and S. Suresh // *Proceedings of the National Academy of Sciences* **104** (2007) 3031.

[26] Z.H. Jin, P. Gumbsch, K. Albe, E. Ma, K. Lu, H. Gleiter and H. Hahn // *Acta Mater.* **56** (2008) 1126.
[27] L. Lu, X. Chen, X. Huang and K. Lu // *Science* **323** (2009) 607.
[28] K. Lu, L. Lu and S. Suresh // *Science* **324** (2009) 349.
[29] J. Wang, N. Li, O. Anderoglu, X. Zhang, A. Misra, J.Y. Huang and J.P. Hirth // *Acta Mater.* **58** (2010) 2262.
[30] X. Li, Y. Wei, L. Lu, K. Lu and H. Gao // *Nature* **464** (2010) 877.
[31] T. Zhu and H. Gao // *Scr. Mater.* **66** (2012) 843.
[32] Y.M. Wang, F. Sansoz, T. LaGrange, R.T. Ott, J. Marian, T.W. Barbee Jr. and A.V. Hamza // *Nature Mater*. **12** (2013) 697.
[33] Z. You, X. Li, L. Gui, Q. Lu, T. Zhu, H. Gao and L. Lu // *Acta Mater.* **61** (2013) 217.
[34] P. Gu, M. Dao and S. Suresh // *Acta Mater.* **67** (2014) 409.
[35] N.F. Morozov, I.A. Ovid'ko and N.V. Skiba // *Rev. Adv. Mater. Sci.* **37** (2014) 29.
[36] I.A. Ovid'ko and A.G. Sheinerman // *Rev. Adv. Mater. Sci.* **39** (2014) 9.
[37] I.A. Ovid'ko, N.V. Skiba and A.G. Sheinerman // *Rev. Adv. Mater. Sci.* **41** (2015) 93.
[38] I.A. Ovid'ko, N.V. Skiba and A.G. Sheinerman // *Rev. Adv. Mater. Sci*. **43** (2015) 38.
[39] Q. Huang, D. Yu, B. Xu, W. Hu, Y. Ma, Y. Wang, Z. Zhao, B. Wen, J. He, Z. Liu and Y. Tian // *Nature* **510** (2014) 250.
[40] P. Gu, M. Dao and Y. Zhu // *Philos. Mag.* **94** (2014) 1249.
[41] H. Zhou, X. Li, S. Qu, W. Yang and H. Gao // *Nano Lett.* **14** (2014) 5075.
[42] I.A. Ovid'ko and A.G. Sheinerman // *Rev. Adv. Mater. Sci.* **44** (2016) 1.
[43] J. Wang and X. Zhang // *MRS Bull.* **41** (2016) 274.
[44] X. Li, M. Dao, C. Eberl, A.M. Hodge and H. Gao // *MRS Bull.* **41** (2016) 298.
[45] N. Lu, K. Du, L. Lu and H.Q. Ye // *Nat. Commun.* **6** (2015) 7648.
[46] Y. Zhu, Z. Li, M. Huang and Y. Liu // *Int. J. Plasticity* **72** (2015) 168.
[47] Z. Horita, K. Ohashi, T. Fujita, K. Kaneko and T.G. Langdon // *Adv. Mater.* **17** (2005) 1599.
[48] R.Z. Valiev and Y.T. Zhu // *Transactions of the Materials Research Society of Japan* **40** (2015) 309.
[49] V. Borovikov, M.I. Mendelev and A.H. King // *Philos. Mag.* **94** (2014) 2875.
[50] L. Velasco and A.M. Hodge // *Acta Mater.* **109** (2016) 142.
[51] N. Li, J. Wang, J.Y. Huang, A. Misra and X. Zhang // *Scr. Mater.* **64** (2011) 149.
[52] B. Predel, in: *Landolt-Börnstein - Group IV Physical Chemistry*, vol. 5d, ed. by O. Madelung, (Springer, Berlin, Heidelberg, New York, 1994), p. 1.
[53] C.S. Hartley, in: *Metallic Alloys: Experimental and Theoretical Perspectives*, ed. by J.S. Faulkner and R.G. Jordan, NATO ASI Series, vol. 256 (Springer, Dordrecht, 1994), p. 271.
[54] A.E. Bayer // *J. Mater. Eng. Performance* **6** (1997) 149.
[55] V.A. Lubarda // *Mech. Mater.* **35** (2003) 53.
[56] J.P. Hirth and J. Lothe, *Theory of Dislocations* (Wiley, New York, 1982).
[57] M.Yu. Gutkin and I.A. Ovid'ko // *Eur. Phys. J.* B **1** (1998) 429.